



This is a repository copy of *No-moving-part hybrid-synthetic jet actuator*.

White Rose Research Online URL for this paper:  
<http://eprints.whiterose.ac.uk/774/>

---

**Article:**

Tesar, V., Hung, C. and Zimmerman, W.B. (2006) No-moving-part hybrid-synthetic jet actuator. *Sensors and Actuators A: Physical*, 125 (2). pp. 159-169. ISSN 0924-4247

<https://doi.org/10.1016/j.sna.2005.06.022>

---

**Reuse**

Unless indicated otherwise, fulltext items are protected by copyright with all rights reserved. The copyright exception in section 29 of the Copyright, Designs and Patents Act 1988 allows the making of a single copy solely for the purpose of non-commercial research or private study within the limits of fair dealing. The publisher or other rights-holder may allow further reproduction and re-use of this version - refer to the White Rose Research Online record for this item. Where records identify the publisher as the copyright holder, users can verify any specific terms of use on the publisher's website.

**Takedown**

If you consider content in White Rose Research Online to be in breach of UK law, please notify us by emailing [eprints@whiterose.ac.uk](mailto:eprints@whiterose.ac.uk) including the URL of the record and the reason for the withdrawal request.



[eprints@whiterose.ac.uk](mailto:eprints@whiterose.ac.uk)  
<https://eprints.whiterose.ac.uk/>

*promoting access to White Rose research papers*



**Universities of Leeds, Sheffield and York**  
**<http://eprints.whiterose.ac.uk/>**

---

This is an author produced version of a paper published in **Sensors and Actuators A: Physical**.

White Rose Research Online URL for this paper:  
<http://eprints.whiterose.ac.uk/774/>

---

**Published paper**

Tesar, V., Hung, C. and Zimmerman, W.B. (2006) *No-moving-part hybrid-synthetic jet actuator*. *Sensors and Actuators A: Physical*, 125 (2). pp. 159-169.  
<http://dx.doi.org/10.1016/j.sna.2005.06.022>

---

# No-moving-part hybrid-synthetic jet actuator

Václav **Tesař**, Chuan-Hsiang **Hung** and William B. **Zimmerman**

Process Fluidics Group, Department of Chemical and Process Engineering, The University of Sheffield, Mappin Street, Sheffield S1 3JD, UK

Received 15 October 2004; revised 9 May 2005; accepted 23 June 2005. Available online 3 October 2005.

## Abstract

In contrast to usual synthetic jets, the “hybrid-synthetic jets” of non-zero time-mean nozzle mass flow rate are increasingly often considered for control of flow separation and/or transition to turbulence as well as heat and mass transfer. The paper describes tests of a scaled-up laboratory model of a new actuator version, generating the hybrid-synthetic jets without any moving components. Self-excited flow oscillation is produced by aerodynamic instability in fixed-wall cavities. The return flow in the exit nozzles is generated by jet-pumping effect. Elimination of the delicate and easily damaged moving parts in the actuator simplifies its manufacture and assembly. Operating frequency is adjusted by the length of feedback loop path. Laboratory investigations concentrated on the propagation processes taking place in the loop.

**Keywords:** *Synthetic jets; Hybrid-synthetic jets; Fluidics; Feedback loop; Acoustic propagation*

## Article Outline

1. Introduction
2. The actuator model
  - 2.1. General
  - 2.2. Amplifier
  - 2.3. Feedback loop
3. Results
  - 3.1. Oscillation frequency
  - 3.2. Modified Strouhal number
  - 3.3. Constant Strouhal number regime
  - 3.4. Constant propagation velocity regime
4. Conclusions
- Acknowledgements
- References

# 1. Introduction

Actuators based on the synthetic jet idea [19] and [25] are currently becoming of increasing importance for a number of applications, especially involving control of flow separation and/or transition to turbulence in internal (e.g. [16]) or external aerodynamics [21], [20], [27] and [28]. They are much more practical and less sensitive to mechanical damage than the initially proposed actuators influencing the flow by mechanical tabs or vanes extended from the wall into the flow. They are also finding use in applications aimed at extremely high power density convective heat and mass transfer between fluid and walls [11], [24] and [30].

Synthetic jets are formed by a periodically alternating inflow into and outflow from a nozzle. They were investigated by the present principal author already more than a quarter of a century ago [4], [6], [7] and [9], mainly with the perspective of using their rectification properties in fluidic pumping [4], [6] and [23]. They were later called “synthetic jets” by Glezer et al. [14], Smith and Glezer [15], Smith and Glezer [18], and Glezer and Amitay [19] the term suggesting their being “synthesised” from individual vortex rings, although this character is there only in a certain range of operating conditions. Synthetic jet actuators are a particularly attractive idea in the context of small scale, microelectromechanical systems (MEMS) – e.g. [17] and [29] – because scaling down is usually associated with decreasing Reynolds number, which decreases efficiency of mixing as well as of convective heat transfer in steady flows. The pulsation associated with of the synthetic jet flows agitates the flowfield and produces effects similar to those of turbulent convection. There are, in fact, some experimental data suggesting that synthetic jets are capable of achieving extreme magnitudes of the thermal power transfer density, unobtainable by any other means, because the pulsation can destroy or reduce the thin insulating layer of stagnant fluid, held at the wall in steady flows. In spite of its minute thickness, this layer has the essential limiting influence on the achievable heat transfer rate, because heat has to cross it by the very ineffective conduction mechanism [24] and [30].

A serious disadvantage of the “pure” synthetic jets, especially in the impingement cooling (or heating) applications, is their re-ingestion of fluid that has already passed over the cooled (or heated) surface. Supply of external, not yet heated (or cooled) fluid is demanded. This is also needed for improvement in the flow manipulation applications, especially beneficial being the additional momentum of the supplied fluid. Recently it became obvious that in several important engineering applications there are definite reasons for using synthetic jets with non-zero nozzle flow rate balance. Usually the balance is positive (more fluid leaving the nozzle per cycle than sucked into it). This method of fluid jet generation – as well as a novel fluid flow actuator – have been investigated by Trávníček et al. [31]. The fluid jets with this type of periodic unsteadiness are called “*hybrid-synthetic jet*” [31]. Simplified cases of harmonic time dependence of the nozzle flow (real wave shapes are usually more complex) for the re-ingesting cases of the periodic jet flow are compared with the mere pulsation in Fig. 1. The word

“synthetic” is retained in the term for the hybrid-synthetic jets because, due to the sign reversal of the flow in the nozzle in each cycle, these flows may retain the typical character of the succession of vortex rings. The actuator described in [31] generated the hybrid-synthetic jet by superimposing on the alternating flow a steady flow component, produced locally by a flow rectification effect using no-moving-part fluidic diodes. If removal of the heat absorbed by the fluid is required, this localised generation may be unsuitable. It may be necessary to bring a replacement fluid to the nozzle by ducts or cavities from more distant locations, even though this eliminates one of the characteristic advantages of synthetic jets, the absence of the ducting and saving the volume (e.g. in an aircraft wing) the duct occupy. However, in the hybrid-synthetic jets this volume may be much smaller than required in the cases of steady flow or the pulsation (Fig. 1) without the re-ingestion.

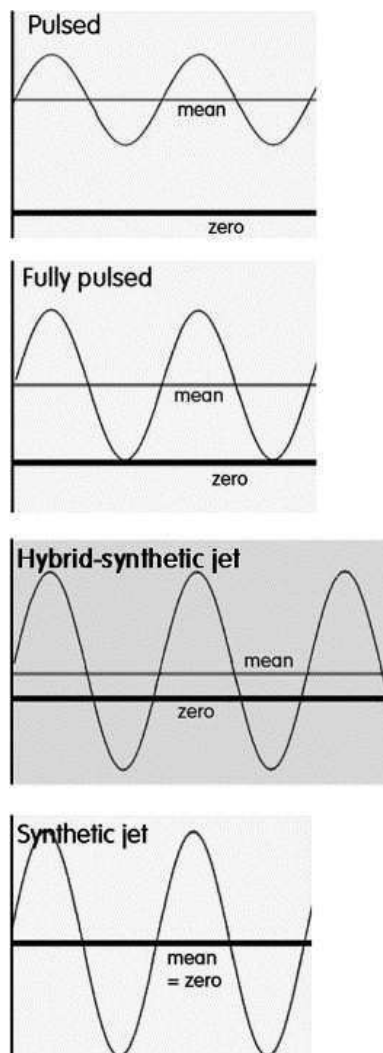


Fig. 1. The present hybrid-synthetic jet case compared with the zero-mean synthetic jet and pulsed flows: time dependences of nozzle flow rates with harmonic oscillation.

In spite of the advantages, a problematic side of current synthetic as well as the newly proposed hybrid-synthetic jets is the generally impractical character of the actuators used to generate the flow. They are now built with moving components like pistons or diaphragms. This complicates both manufacturing and assembly. The moving devices are delicate and easily damaged, and generally exhibit a limited life span. They cannot operate at high temperatures required in some high thermal power density applications. Electromagnetic drivers used to move the pistons are heavy. Electrostriction and piezoelectric principles have difficulties in producing sufficient volume changes.

Flow control using no-moving-part fluidic oscillators, without the problems associated with of mechanical oscillation generators, has been known since 1970s [3] and was recently reviewed in the survey by Raman and Cain [22]. However, the fluidic oscillators have been always intended as mere distributors of the supplied flow alternatively into two exit nozzles—or more often without the exit nozzles as devices superimposing pulsation (Fig. 1) on an otherwise steady flow, thereby, e.g. influencing the aerodynamic properties of jets [5]. There was never an idea of utilising the jet-pumping effect inside the fluidic oscillator for generating the suction into the exit nozzle for a part of the oscillation cycle. This novel way of generating the hybrid-synthetic jets is the subject of the present paper.

## **2. The actuator model**

### **2.1. General**

The basic idea of the described actuator is shown schematically in Fig. 2. The alternating flow in two exit nozzles A and B is generated by a no-moving-part actuator driven by supplied air flow. The actuator is extremely simple, consisting of a specially shaped cavity in which the periodic aerodynamic processes take place. Essentially, the actuator consists of two components: (a) a small fluidic flow control valve of the type described, e.g. in [2], [10] and [12] or [13], and (b) feedback loop channel, the flow in which de-stabilises the valve and produces self-excited oscillation [1]. To be able to activate the feedback flow, the valve has to exhibit amplification properties—a higher than unity flow and/or pressure gain between its input control terminals X and the output terminals Y. The output flow is provided from the supplied steady flow, brought into the supply nozzle through the supply terminal S. In the present case, the fluidic amplifier valve is of the diverter type. The supplied flow is not turned down by the control action, but diverted into one of the two output terminals,  $Y_1$  and  $Y_2$ . Each of them is connected to one of the two exit nozzles, A and B. The time-mean flow rate in each nozzle is positive: more flow issues in the outflow phase than is sucked in during the following inflow suction phase of the cycle. The actuator drives not a single nozzle but two nozzles operating in opposing phases—suction in nozzle A is simultaneous with outflow from the other nozzle B. Availability of two phase-shifted exit flows is an advantage for some applications.

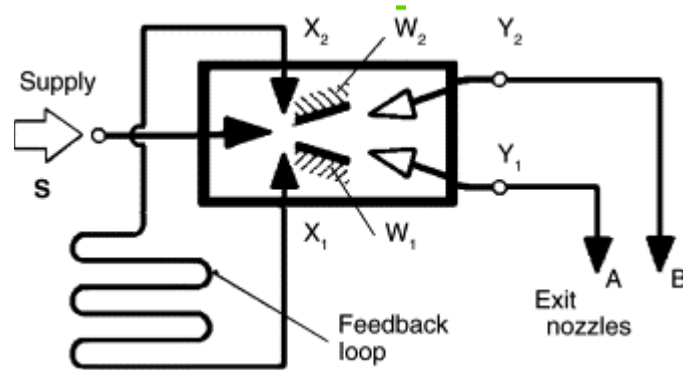


Fig. 2. Schematic representation of the fluidic oscillator: a jet-deflection diverter type fluidic bistable amplifier is provided with feedback loop connecting the two control terminals  $X_1$  and  $X_2$ . Black triangles: nozzles, white triangles: diffusers.

The oscillating-flow valve under investigation is actually a scaled-up laboratory model of the proposed future final device. The scaling up in the present case is intended not only to simplify the study of the actuator properties but also to make possible use of the model in wind tunnel experiments scaled up to make easier a smoke visualisation and PIV measurements of the controlled external near-wall flows. The model was designed to operate with  $d_n = 6$  mm dia exit nozzles (A and B), while the future final version of the actuators used in flight vehicles are to have five times smaller exit diameter  $d_n = 1.2$  mm. The hybrid-synthetic jet to be generated by the flight vehicle version of the actuator is required to operate at a frequency of  $f = 150$  Hz. Conditions in periodic unsteady flows are governed by the Stokes number similarity: if the scaled up model is to behave in a hydrodynamically similar manner, its operating Stokes number:

$$Sk = \frac{fd_n^2}{\nu} \quad (1)$$

where  $\nu$  is the (kinematic) fluid viscosity – is to be the same. For air at the usual laboratory conditions, the above-mentioned actuator is to operate at  $Sk = 13.76$ . For the five times scaled up model, the same value of  $Sk$  requires the operating frequency to be very low, at only  $f = 6$  Hz. Experimental results prove (cf. Fig. 13) that the model is actually capable of operating in sustained oscillation across a wide frequency spectrum, from  $\sim 1$  to  $\sim 200$  Hz, which (with some caution) may be interpreted as the range from  $\sim 25$  Hz to  $\sim 5$  kHz in the five times smaller unit.

## 2.2. Amplifier

The amplification property is due to the capability of diverting the jet leaving the supply nozzle by the action of much weaker control flows, brought into the control terminals  $X_1$  and  $X_2$ . In the tested model the steady state flow amplification gain is approximately 14.5. This means that for deflecting the flow from one output terminal to the other it is sufficient to apply a control flow of approximately 7% of the supplied air

flow. In actual operation, the flow in the valve is switched by incoming pulses, which – owing to their sudden shock character – may be even weaker.

The amplifier exhibits bistability: if there is no acting control signal, it remains in one of two alternative stable states. This is achieved by using the Coanda effect of jet attachment to walls. There are two attachment walls,  $W_1$  and  $W_2$  (Fig. 2) placed symmetrically on both sides of the path of the main jet, which is formed by the supply flow issuing from the supply nozzle. The jet may attach equally well to either one of the two walls, which keep it deflected and guide it into one of the two collectors, connected to the output terminals  $Y_1$  and  $Y_2$ . Shown in Fig. 3 there are computed pathlines in the valve for the state with the jet guided into the output terminal  $Y_2$ . The jet-pumping effect of the entrainment into the jet should be noted: the output mass flow rate  $\dot{M}_{Y_1}$  passing through the output terminal  $Y_1$  is negative. It is useful to relate its value to the magnitude of the supplied mass flow rate  $\dot{M}_s$ ; in the particular case of the valve geometry shown in Fig. 4 the steady-state computed relative value:

$$\mu_{Y_1} = \frac{\dot{M}_{Y_1}}{\dot{M}_s} \quad (2)$$

was

$$\mu_{Y_1} = -0.17 \quad (3)$$

a small value (suction flow maxima in oscillation regime are actually higher) but enough to terminate the previous positive outflow and generate a vortex ring downstream from the nozzle A. A short flow pulse admitted into the control terminal  $X_2$  then suffices for switching the jet so that it is directed into the other output terminal  $Y_1$ .

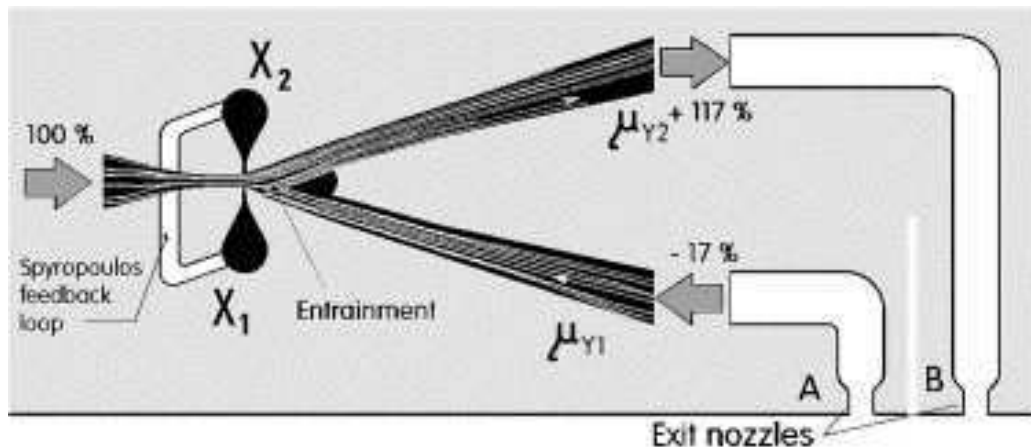


Fig. 3. The entrainment into the jet directed towards the nozzle B in the amplifier generates a return flow into the exit nozzle A – changing their role in the next half-cycle. This way, the flows from the nozzles generate the desired hybrid-synthetic jets. In the oscillatory regime, the relative return flows are much larger than the values shown here obtained by steady-state computation.

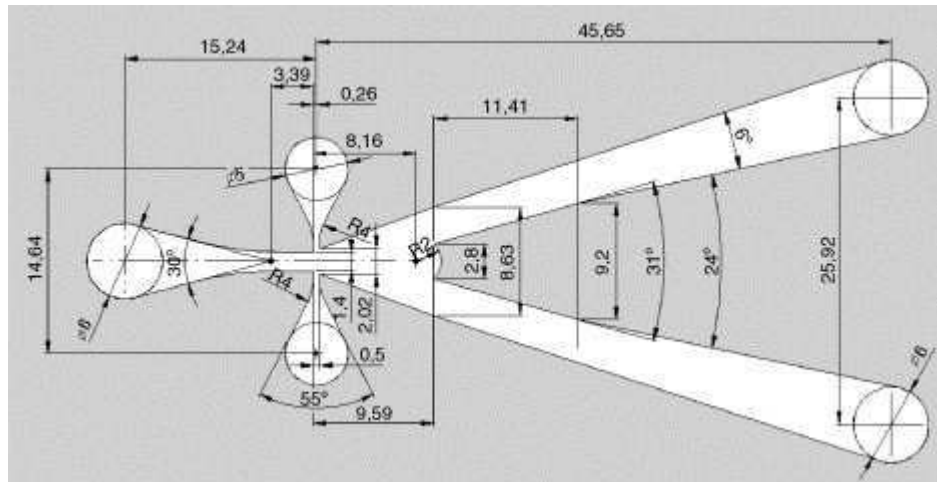


Fig. 4. Geometry of the amplifier, derived from the successful geometry [A] used by Tesař [1] and later Perera and Syred [7].

The geometry specified in Fig. 4 is symmetric and planar—all cavities forming the amplifier are of the same depth. It was designed on the basis of an earlier favourable experience with the geometry [A] in [2] and later successfully used by Perera and Syred [8]. Remarkable detail is the positive internal feedback created by the concave bi-cuspid shape of the splitter between the two collectors. The amplifier was made by laser cutting the contour shape in polymethylmetacrylate (Perspex) sheets, of 1.2 mm thickness. To obtain a higher nozzle aspect ratio as well as an exit cross-section compatible with the required 6 mm dia exits, the valve body was made by stacking five sheets. The stack was clamped between thick Perspex top and bottom cover plates, as shown in Fig. 5. The output terminals of the same 6 mm diameter as well as the supply terminal of the same size, together with the smaller 5 mm dia control terminals, were all made as drilled holes in the bottom cover plate.

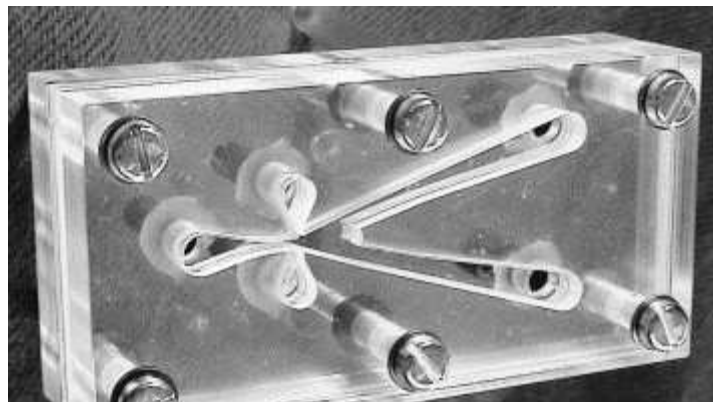


Fig. 5. Photograph of the assembled amplifier as used in the experimental investigations. The stack of sheets with laser-cut cavities was clamped between thick transparent cover plates.

The performance of the amplifier valve was investigated by a series of numerical flowfield computations using a standard commercial CFD software FLUENT 6. The computation domain, fully three-dimensional, corresponded to the test model. It was discretised using an unstructured grid of 69,501 tetrahedral finite volumes (18,715 triangular wall faces). The computations used standard 2-equation turbulence model with RNG handling of low turbulence Reynolds numbers. The investigations were focused on ascertaining the controllability, which was the only problem encountered earlier with the geometry [A] (which required narrowing the control nozzle exit during its development as described in [2]). It should be perhaps mentioned that the rather small, 0.5 mm control nozzle width of the present model were initially considered too small for reproducible manufacturing by the laser cutters. A possibility of increasing the width to 0.7 mm was investigated, but the results of this change were disappointing, indicating again advisability of small control nozzle widths.

Steady-state computational results (with the 0.5 mm control nozzle width) in Fig. 6, Fig. 7, Fig. 8 and Fig. 9 show details of the flow control by switching. In Fig. 6, the switching process is presented (symbols denoting individual computed states) in terms of the flow transfer characteristic—the dependence of the relative output flow  $\mu_{Y_1}$  (Eq. (2) in the terminal  $Y_1$  on the relative control flow rate in the terminal  $X_1$ ):

$$\mu_{X_1} = \frac{\dot{M}_{X_1}}{\dot{M}_s} \quad 4)$$

which is first increasing and then decreasing, maintaining constant supply mass flow rate  $\dot{M}_s$  (and hence constant Reynolds number  $Re$ ). The two exit nozzles issue into the same space so that the pressure difference  $\Delta P_Y$  between the amplifier outputs is constant and equal to zero. In the state A, with at the beginning zero control flow and the supplied air flow directed into the output terminal  $Y_1$  the computed flowfield is shown in Fig. 7. Note that in this state the relative output flow rate in Fig. 6 is

$$\mu_{Y_1} = 1.17 \quad (5)$$

larger than 1.0 because of the added inflow from  $Y_2$  given (its magnitude given by Eq. (3) — note, however, the opposite position of the jet). Subsequent increase of the control flow  $\dot{M}_{X_1}$  has little effect, just slightly decreasing the jet pumping into  $Y_2$ . The small influence is mainly because any tendency towards deflection of the jet into  $Y_2$  is countered by the positive internal feedback, provided by the standing vortex trapped between the cusps of the splitter. This is shown in the state B immediately before the switching in Fig. 8. The switching takes place when the further increase of the control flow rate to  $\mu_{Y_1} = -0.17$  overcomes the combined action of the Coanda effect and the stabilising internal feedback. In the next computed state C, Fig. 9, the jet from the supply nozzle is already attached to the other attachment wall. The flow through the output terminal  $Y_1$  is now negative and it should be noted that its magnitude is due to additional jet-pumping effect of the control flow — larger than the value given by Eq. (3).

Subsequent further increase of the control flow rate brings no qualitative changes. The jet pumping effect is seen in Fig. 6 to grow, up to about  $\mu_{Y1} = -0.3$ . This is an important fact: in the oscillatory regime, with large control flows, the effective return (suction) flow in the exit nozzles are substantially higher than what might be expected by considering the zero control flow values in Fig. 3.

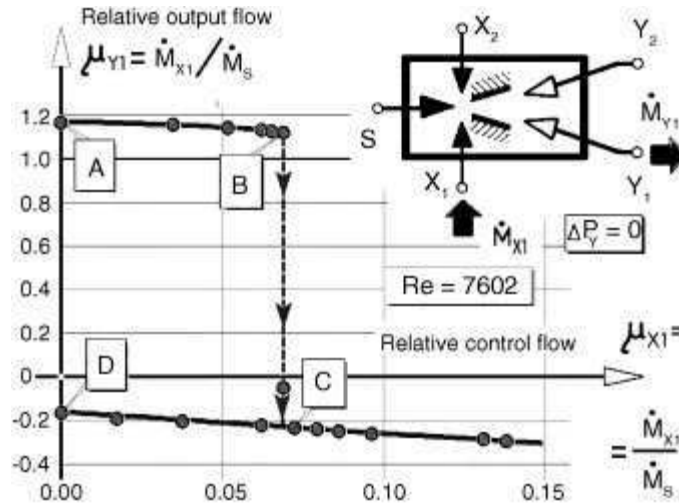


Fig. 6. Flow transfer characteristic of the amplifier in relative co-ordinates: the response to the control signal admitted to only one control terminal  $X_1$ . Switching takes place when the control flow  $\dot{M}_{X1}$  reaches  $\sim 7\%$  of the supply mass flow rate  $\dot{M}_S$ .

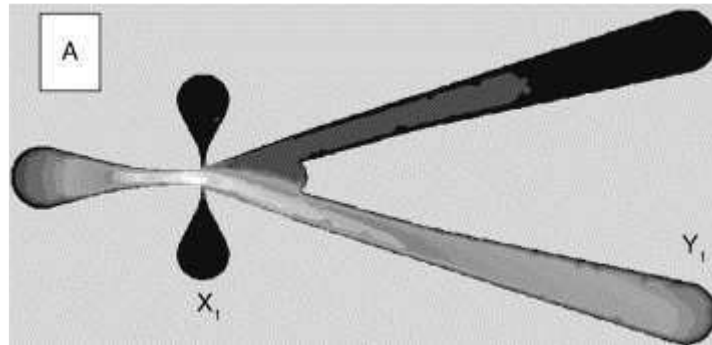


Fig. 7. Computed velocity distribution in the midplane (at  $h/2 = 3$  mm from the bottom of the cavities) with no control flow-state A in Fig. 6. Lighter shades of grey (rendering of the original colour coding) correspond to higher absolute velocity.

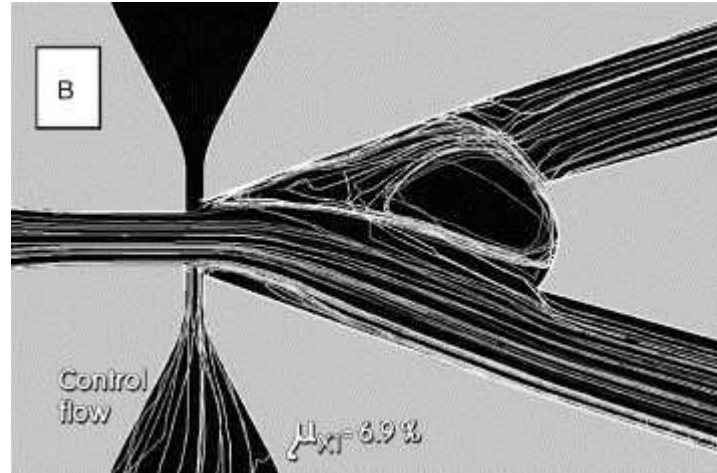


Fig. 8. Pathlines of flow in the state B of Fig. 6. The cusped splitter nose generates an internal positive feedback loop resisting the switching.

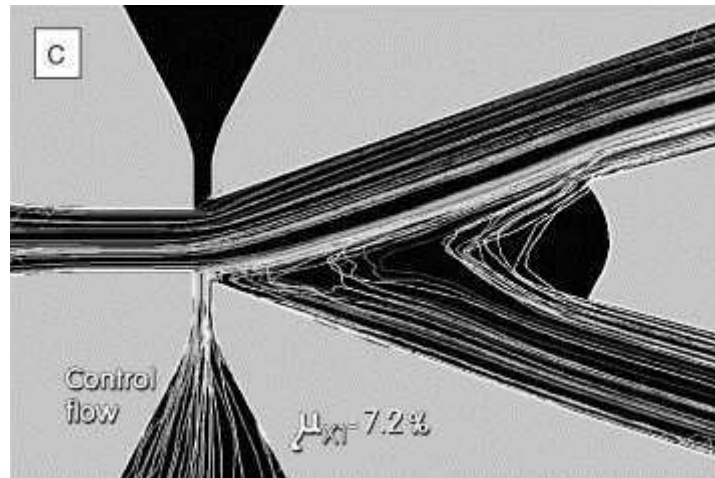


Fig. 9. Numerically computed pathlines in the state C of Fig. 6. The control flow has overcome the internal feedback and the jet is switched to the other attachment wall.

When the control flow is then decreased, there is, of course, no return to the state C. Instead, the state D shown already in Fig. 3, with the smaller suction rate  $\mu_{Y1} = -0.17$ , is finally reached when the control flow returns to zero.

### 2.3. Feedback loop

To produce the oscillation, the amplifying valve is provided with negative feedback loop arranged to be more powerful than the stabilising positive internal feedback. There is no classical connecting of the output and control terminals. The disadvantage in the case of the present amplifier with two input as well as two output

terminals would be the necessity of providing two such loops. A simpler version of feedback actually used, as shown in Fig. 10, uses the single feedback loop connecting the two control terminals  $X_1$  and  $X_2$ . The feedback loop has to introduce a delay into the feedback signal path. With the simple connecting tube (without accumulation in a chambers), the cause of the delay is mostly the fluid inertia. Another mechanism is a delay due to the finite propagation time of acoustic waves in the tube. In the present case, the results indicate the presence of both mechanisms.

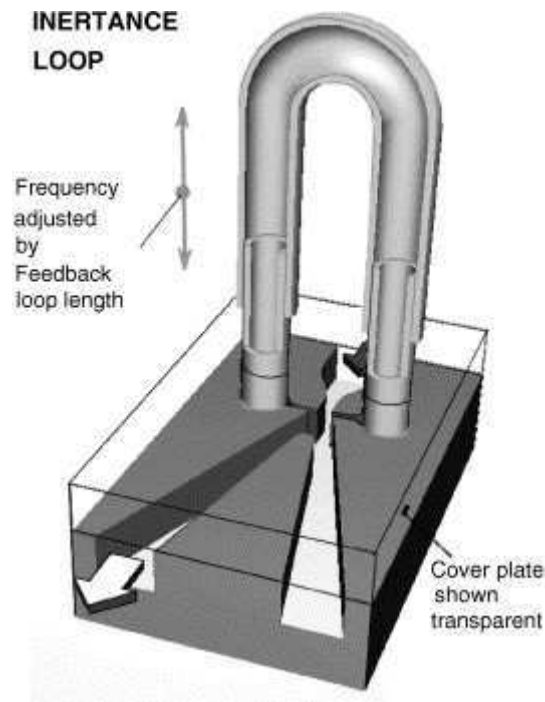


Fig. 10. The feedback loop converts the amplifier into an oscillator by connecting its two control terminal with the feedback loop tube. The “trombone” frequency adjustment may be useful for fine tuning; in the present experiments the tube length was adjusted by gradual cutting.

The feedback action is based on the pressure difference between the two control nozzle terminals  $X_1$  and  $X_2$  caused by the entrainment into the jet. This is the cause of the Coanda effect that keeps the jet at its attachment wall. The pressure is lower at the side where the attachment wall prevents a flow of additional outer fluid into the entrainment region. If connected by the feedback loop, the difference gives rise to a fluid flow in the loop towards the lower-pressure control nozzle. This flow gradually gains a momentum sufficient for driving a substantial control flow into this nozzle. Because of the amplification properties of the valve, this control flow suffices to switch the jet to the opposite attachment wall. The pressure difference between the control terminals  $X_1$  and  $X_2$  caused by the entrainment into the jet then changes sign, tending to reverse the flow direction in the loop. Because of fluid inertia, however, it takes some time for the fluid in the loop channel to come to a stop and to begin flowing back. This provides the phase

delay. The jet remains for a certain short time attached to the opposite attachment wall, sufficiently long to produce the inversed pressure levels in the control nozzles. Then, however, the reverse flow in the feedback loop increases and when it reaches the 7% limit, switches the jet back to its original position. The oscillation cycle then can start anew.

Because of the decisive importance of the duration of the cycle of the delay in the feedback loop, it is easy to adjust the frequency of generated oscillation by changing the loop length. One possibility is shown in Fig. 10. In the present case, however, the requirement of the very low frequency led to very large feedback loop tube lengths of the order of metres. The “trombone” change of length would be impractical. Instead, in the laboratory experiments, a Tygon tube of original full 52 m length obtained from supplier was gradually cut to shorter lengths, ending at 1 m. To investigate the effect of tube diameter, the procedure was repeated with four tubes, of 2.5, 4, 5, and 10 mm i.d. The cross-sectional areas of these tubes were  $\varphi$ -times larger than the control nozzle exit cross-section, according to the accompanying table. Most results presented here are for  $d = 10$ , but effect of  $d$  was interesting—its size can influence substantially the signal propagation velocity in the loop.

$d$ (mm)	Area ratio ( $\varphi$ )
2.5	1.64
4	4.19
5	6.54
10	26.18

## 3. Results

### 3.1. Oscillation frequency

The oscillator was found to generate the oscillations reliably across a wide range of conditions. The output was picked up by piezoelectric pressure transducer and monitored on an oscilloscope. Fig. 11 and Fig. 12 present typical example of oscilloscope traces obtained in the experiment with the largest, 10 mm i.d. feedback loop tube. As seen in Fig. 11, the waveshapes at low frequencies were nearly rectangular and very regular. The rectangularity is due to the jet in the valve remaining attached at one of the attachment walls until the switching occurs. However, as the frequency increased with shortening the tube length  $l$ , the high-frequency components of the spectrum became progressively more damped until the waveshapes approached (but never reached) the simple harmonic oscillation as shown schematically in Fig. 1. The scatter superimposed on the rectangular shape in Fig. 11 was partly due to transition phenomena (after each

switching) in the sensors and signal processing devices and partly caused by flow turbulence. Comparison with Fig. 12 provides a useful idea about what is obtained with a decreasing supply flow rate. Apart from the smaller oscillation frequency, there was a recognisably lower level of high-frequency turbulence. The relative magnitude of the low-frequency noise is, however, roughly the same. The noise visible in Fig. 11 and Fig. 12 made the measurement of the main variable of interest, the oscillation frequency  $f$ , somewhat imprecise. It was hence decided to evaluate the frequency  $f$  as the inverse of the mean oscillation period  $\Delta t$  measured in the oscilloscope records.

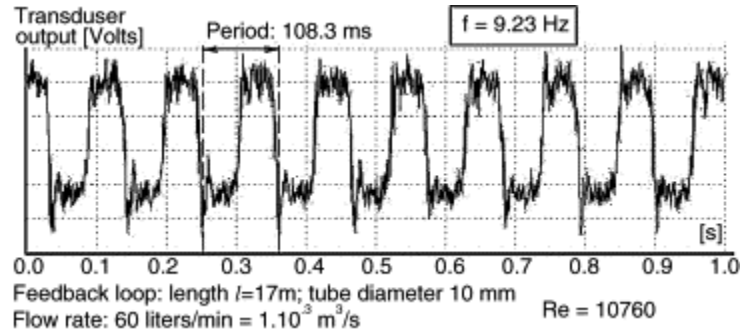


Fig. 11. An example of a typical oscilloscope record of generated oscillation with 10 mm i.d. tube loop.

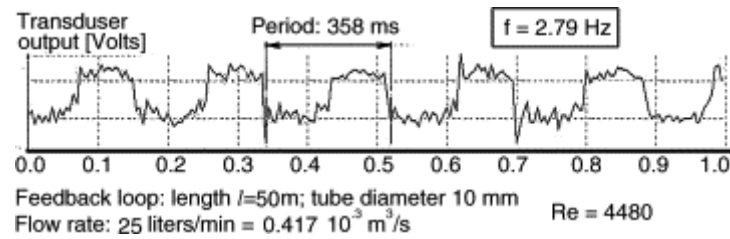


Fig. 12. Another example of the oscilloscope trace—with the same 10 mm i.d. loop at a lower Reynolds number. Absolute magnitude of the noise is lower, but also the pulsation is weaker (requiring increased oscilloscope magnification). Resultant signal/noise ratio is nearly the same as in Fig. 11.

The experiments were performed with air. At each of the four tube diameters  $d$ , the tube length  $l$  was gradually decreased. With each length  $l$ , the oscillator was supplied by gradually increased volume flow rate in eight steps from 10 to 80 l/min. This corresponded to the supply nozzle exit Reynolds numbers from  $Re = 1790$  (at the very beginning of transition into turbulence in the issuing jet) to  $Re = 14,340$  (fully turbulent jet). Fig. 13 shows that oscillation frequency  $f$  increased in inverse proportion to the decreased length  $l$  of the feedback loop. The dependence on flow rate was found more complicated. The usual property of many self-excited aerodynamic oscillations is a constant, Reynolds number independent value of Strouhal number  $Sh$ ; which in fluidics is usually evaluated as

( $b$  is the supply nozzle width and  $w$  is the supply nozzle bulk exit velocity). The value is plotted in Fig. 14 (for the data from Fig. 13) as a function of the supply nozzle Reynolds number. Somewhat disappointingly, this non-dimensionalisation did not lead to a simple overall picture.

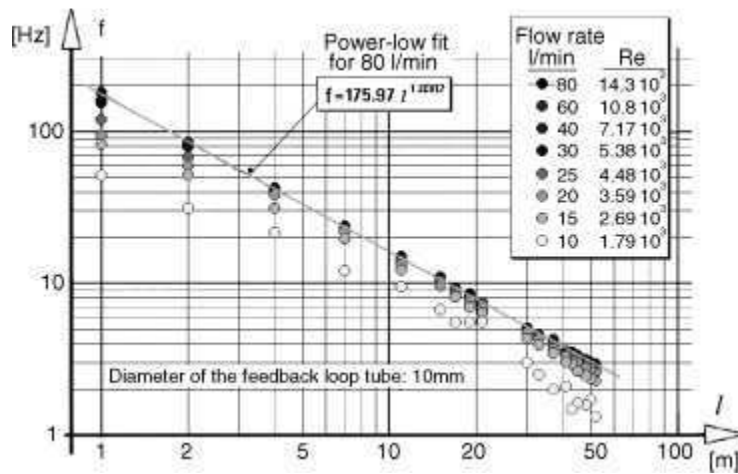


Fig. 13. The frequency vs. loop length dependences obtained with the 10 mm dia loop tube at different supply flow rates. The power law fit exponent near to 1.0 suggest that the frequency is simply inversely proportional to the feedback loop length  $l$ .

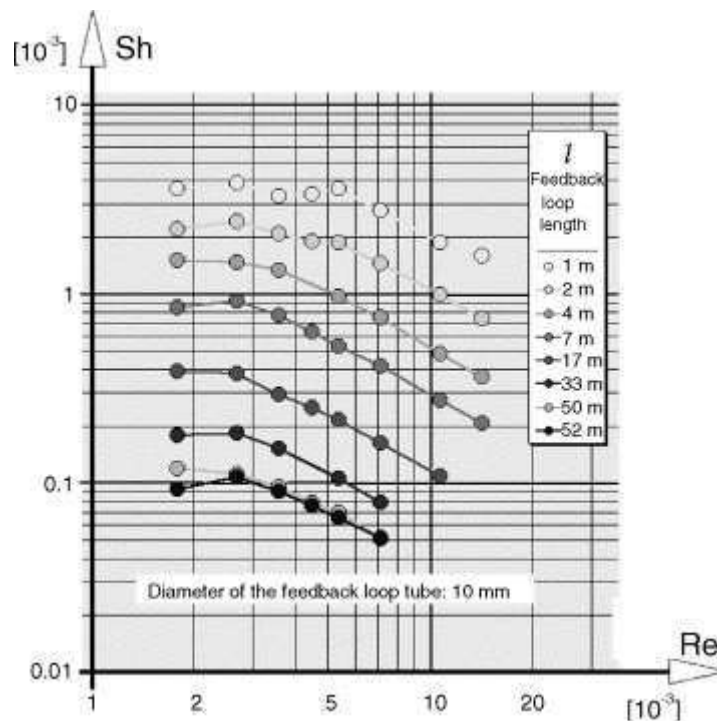


Fig. 14. The experimental results obtained with the 10 mm dia loop tube at different supply flow rates re-plotted in terms of the Strouhal number  $Sh$  as a function of Reynolds number  $Re$ .

### 3.2. Modified Strouhal number

As a step towards finding an invariant of the investigated phenomenon, it seemed reasonable to multiply  $Sh$  defined in Eq. (6) by the length  $l$  to utilise the inverse proportionality  $f \sim 1/l$  of Fig. 13. To retain the non-dimensionality,  $Sh$  was multiplied by the relative length  $l/b$ , leading to modified Strouhal number evaluated from the tube length  $l$  as the characteristic dimension. Indeed, the result in Fig. 15, re-plotting the data from Fig. 14, is a welcome simplification. It should be noted that the modified Strouhal number in Fig. 15 is actually multiplied by a factor of 2.0. This has no effect on the character of the dependence, but brings an interesting interpretation possibility. This is based on an observation that the jet switching in the valve is a fast process so that the oscillation period  $\Delta t = 1/f$  measured in the oscilloscope records (Fig. 11 and Fig. 12) is almost equal to two propagation times of the switching signal in the feedback loop. The available frequency and length data make possible the following rough estimation of the propagation velocity  $w_a$ :

$$w_a = \frac{2l}{\Delta t} = 2fl \quad (7)$$

of the signal in the tube. The modified Strouhal number using the length  $l$  as the characteristic dimension may be therefore interpreted (Fig. 15) as the ratio of this propagation velocity and the nozzle exit velocity. The result is an inverse to the common definition of Mach number:

$$Ma = \frac{w}{w_a} \quad (8)$$

$w$  is the exit velocity and  $w_a$  is the acoustic propagation velocity. Of course, taking the velocities from different locations has nothing to do with standard Mach numbers and the quantity serves here merely as a short-hand notation extending the  $Ma$  concept beyond the boundaries of its standard usage.

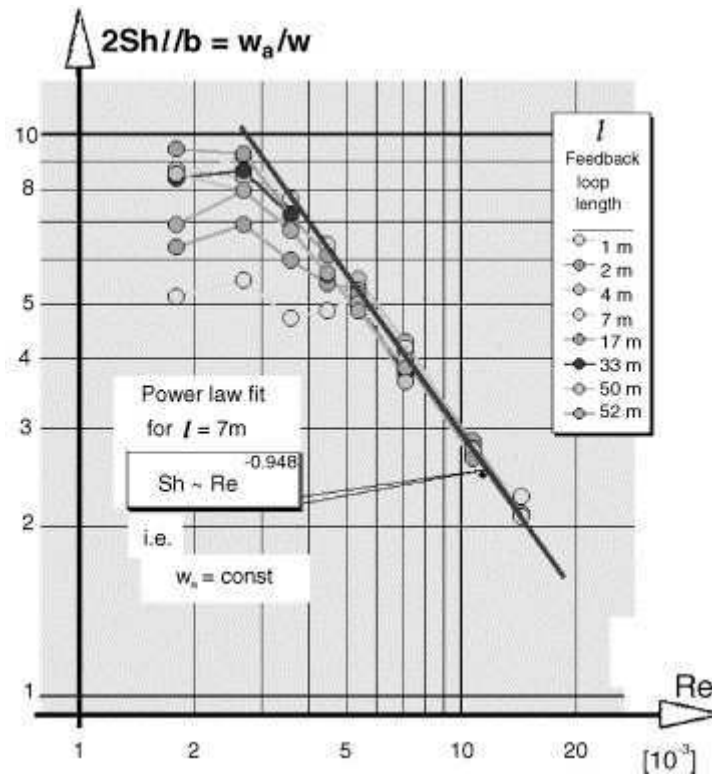


Fig. 15. Another re-plotting of the results from Fig. 13 using the modified Strouhal number. The data suggest there are two different regimes: one at low  $Re < 3000$  and the other at high  $Re$ .

Considering the overall picture obtained with the area ratio  $\varphi = 26.18$  feedback tube in Fig. 15 – with the other tube diameters the overall character is analogous – it is apparent that the results conform to the usual idea of Reynolds number independent Strouhal number only at very low  $Re$  end. The modified Strouhal number there still recognisably depends on the tube length  $l$ .

On the other hand, there is a distinctly different regime at the high  $Re$  end of the investigations. Here, the dependence on the length  $l$  disappears. The data there admit a power-law fit, in Fig. 15 made for tube length  $l = 7$  m. The value of the exponent very near to 1.0 suggests that neglecting the experimental inaccuracy, there is

$$\frac{1}{Ma} \sim \frac{1}{Re} \quad (9)$$

which by cancellation of  $w$ , means a constant propagation velocity:

$$10)$$

### 3.3. Constant Strouhal number regime

At the low  $Re$ , perhaps approximately  $Re < 3500$ , which may be plausibly interpreted as the regime of laminar character of the jet issuing from the supply nozzle, at least in the vicinity of the control nozzles, the modified Strouhal number is apparently independent of  $Re$ . The extent of Reynolds numbers in Fig. 16 is too short to make this fully convincing, but the constancy is supported by measurements with different area ratio  $\phi$  feedback tubes, as may be seen from the linear growth of frequency with the supply mass flow rate in Fig. 20. For long tubes,  $l > 5$  m, the modified Strouhal number is also practically independent of the loop length  $l$ . This is documented in Fig. 17. For shorter lengths ( $l < 5$  m) the low  $Re$  values exhibit a weak growth with lengths  $l$ , the modified Strouhal number being there roughly proportional to  $\sqrt{\sqrt{l}} = l^{1/4}$ . This, however, is the region of short signal propagation times where the switching time inside the valve may become a non-negligible part of the overall delay in the feedback that governs the oscillation frequency. As a result, the dependence in Fig. 17 may be an apparent effect caused by the simplification in deriving Eq. (7).

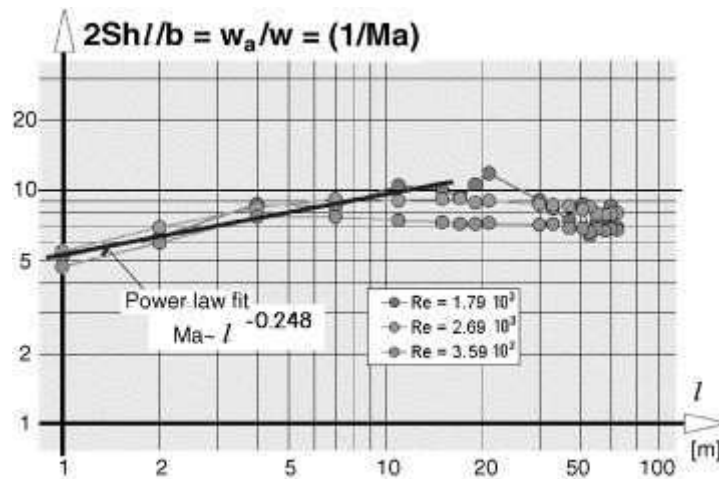


Fig. 16. The data for low  $Re$  (here  $Re < 4000$ ) from Fig. 15 show the modified Strouhal number practically independent of loop length  $l$ , for long tubes  $l > 5$  m. For short lengths ( $l < 5$  m) there is a recognisable growth roughly proportional to  $l^{1/4}$ .

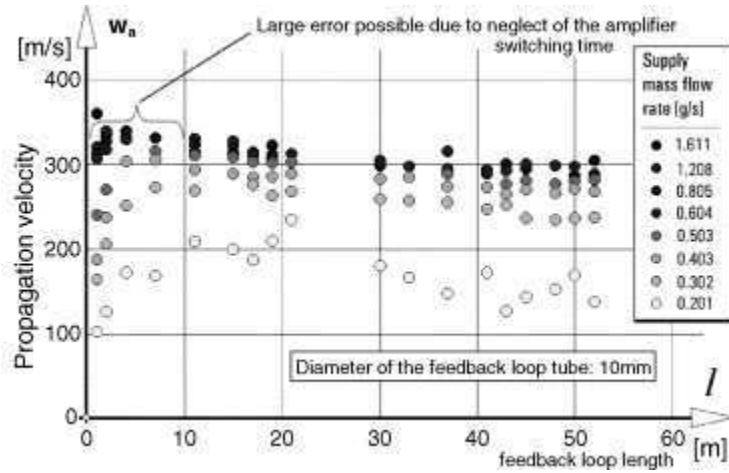


Fig. 17. Velocity of the signal propagation  $w_a$  (approximately evaluated) in the feedback loop is near to the speed of sound. In the high Reynolds number regime  $w_a$  is constant—here seen to be practically independent of the loop length  $l$ .

### 3.4. Constant propagation velocity regime

In this regime, the propagation velocity  $w_a$  evaluated by the approximate Eq. (7) is a constant not only independent of the flow rate through the valve (Fig. 17 and Fig. 18) but also of the other varied parameter, the feedback loop length  $l$  (Fig. 17). The transition into this regime, plotted in terms of the flow rate in Fig. 18 or in terms of  $Re$  in Fig. 19, resembles similar dependences found in aeroelastic phenomena with lock-in to elastic resonance. A typical example may be, e.g. fluid flow driven vibration of an elastically supported cylinder in cross-flow, which oscillates at the vortex shedding frequency increasing with flow velocity unless the frequency is near to the resonant frequency determined by the cylinder mass and elastic constant of the support, which then becomes dominant causing the oscillation to be, in a certain range, insensitive to velocity changes. This analogy suggests quite strongly that there is a similar cause, a resonant phenomenon, behind the observed range of insensitivity to the flow rate changes. The propagation velocity values of  $w_a$  in this insensitive region in Fig. 17 and Fig. 19 are so near to the speed of sound:

$$w_{a,ad} = \sqrt{\alpha r T} \quad (11)$$

$r$  (J/kgK) is the gas constant of air and  $T$  (K) temperature, that there is little doubt about the resonance is an acoustic one. Eq. (11), of course, is valid for adiabatic propagation in unbounded space. In a tube, the temperature changes associated with the compression in the propagating sound wave do not affect a thin thermal boundary layer at the tube wall. The temperature in the layer remains near to the original temperature of the wall. A very simple model of the compression process  $Pv^k = \text{const}$  may assume adiabatic core with polytropic exponent  $k = \gamma$  and the isothermal layer with  $k = 1$ . Alternatively, one may introduce a global polytropic exponent for the whole tube, involving the combined

effect of these two components and having there fore values between 1 and  $\infty$ . Obviously, if the tube diameter  $d$  is smaller, the relative magnitude of the isothermal layer volume is larger and the overall exponent decreases, in turn decreasing the propagation velocity:

$$w_a = \sqrt{krT} \tag{12}$$

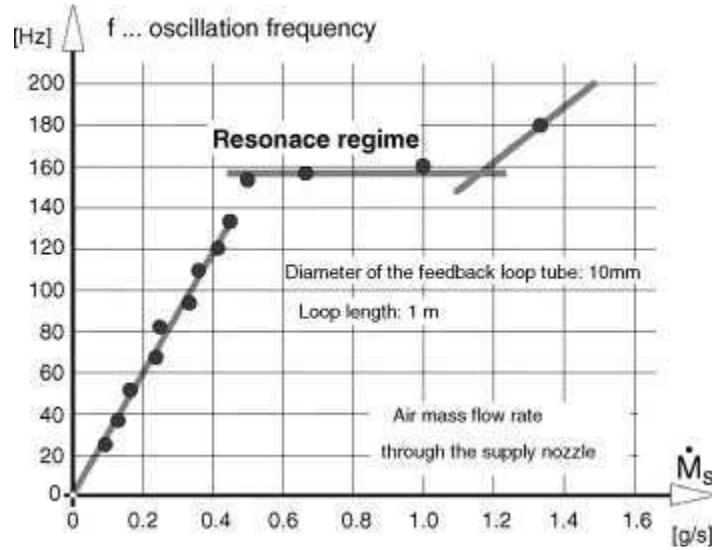


Fig. 18. Constant  $Sh$  linear growth of oscillation frequency  $f$  with flow rate at low  $Re$  is replaced at higher flow rates by constant-frequency resonance. Some data suggest continuation of the linear growth beyond the resonant lock-in.

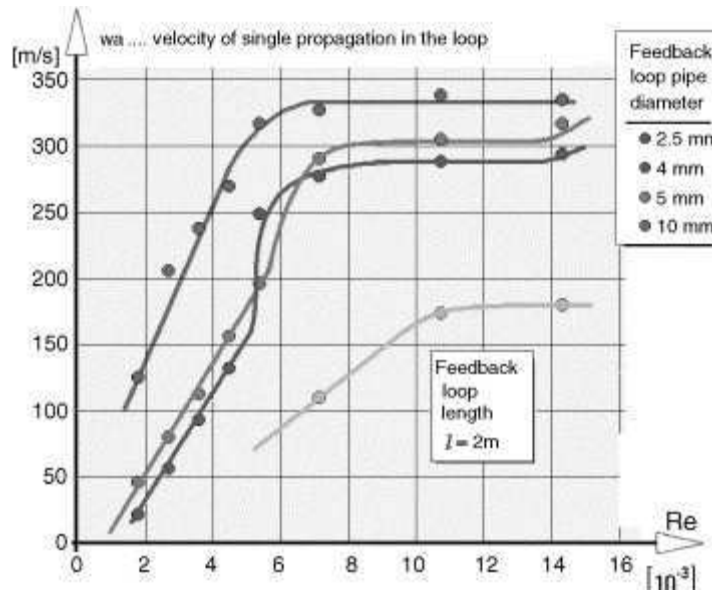


Fig. 19. The propagation velocity (again evaluated approximately, neglecting the switching time in the amplifier) for different feedback tube diameters show the similar transition into the regime B, locked-in to what is apparently an acoustic resonance.

Indeed, the propagation velocity in Fig. 19 is seen to be smaller. It is plotted in Fig. 20 in nondimensional presentation, as a dependence on the feedback loop tube Stokes number:

$$Sk_t = \frac{fd^2}{\nu} \quad 13)$$

showing how the heat transfer phenomena (thermal boundary layer) in the small diameter tubes can substantially decrease the propagation speed below the adiabatic value. The results, despite the approximative nature of Eq. (7), are in remarkable agreement with values obtained by much more sophisticated propagation measurement methods.

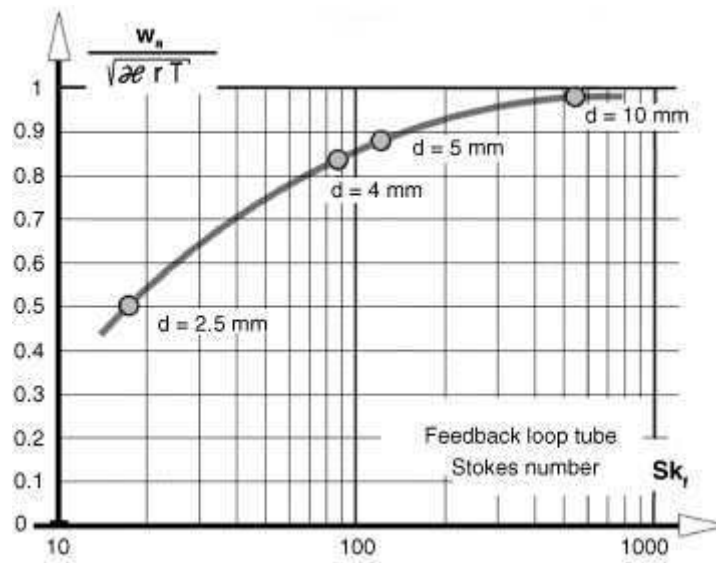


Fig. 20. Dependence of the propagation velocity in resonant conditions in the feedback loop tube on Stokes number for different tube diameters  $d$ .

## 4. Conclusions

Control of flow and/or heat and mass transfer by the hybrid-synthetic jets operates with flow pulses of higher magnitude than the supplied time-mean flow rate—thus reducing the requirements placed on the supply ducting, while character of succession of ring vortices is the same as in the standard zero time-mean synthetic jets (e.g. [26]). The continuous exchange of fluid is a particular advantage for synthetic jet operations in stagnant or low velocity outer conditions, especially if these involve increased temperature.

In this paper, the idea of generating the hybrid-synthetic jets by the no-moving-part fluidic oscillator was experimentally verified on a laboratory model and proved to be

a sound one. The actuator eliminates the problems associated with bringing to it the driving electric current. It is easy and inexpensive to manufacture, lightweight and yet robust and resistant to adverse conditions. It lends itself to modern manufacturing methods (laser cutting the present model form, etching in the intended small scale). It needs no maintenance and when made from suitable materials may resist even extremely high temperatures, acceleration and radiation environment.

From theoretical point of view, it was surprising to find that in the operating range of interest the processes are apparently undergoing a transition between two different regimes, revealing quite complex underlying aerodynamic mechanisms taking place inside what is a simple constant cross-section feedback loop tube.

## Acknowledgments

The stay of the principal author (V. Tesař) at the University of Sheffield in the course of the development of the actuator was supported by funds granted by EPSRC to W.J.B. Zimmerman. The authors are grateful to Dr. Shan Zhong, School of Mechanical, Aerospace, and Civil Engineering, University of Manchester, for her interest and practical testing of the actuator in her wind tunnel investigations.

## References

- [1] C.E. Spyropoulos, A Sonic Oscillator, in: Proceedings of the Fluid Amplification Symposium, vol. III, Harry Diamond Laboratories, Washington, D.C., 1964, pp. 27–51.
- [2] V. Tesař, A mosaic of experiences and results from development of high-performance bistable flow-control elements, *Proceedings of the Conference on Process Control by Power Fluidics* Sheffield, UK (1975).
- [3] H. Viets, Flip-flop jet design, *AIAA J.* **13** (1975), pp. 1375–1379.
- [4] V. Tesař, Pump or blower, in particular for transporting difficult-to-pump fluids-in Czech, Czechoslovak Certificate of Authorship No. 192 082, April 1976.
- [5] M. Favre-Marinet and G. Binder, Structure des jets pulsants, *J. Mécanique, Théorique Appl.* **18** (1979), p. 357.
- [6] V. Tesař, Fluidic pump driven by alternating air flow, *Proceedings of the PNEU-HIDRO'81 – IV. Colloquium on Pneumatics and Hydraulics* Győr, Hungary, September (1981).
- [7] V. Tesař, Fluidic jet-type rectifier: experimental study of generated output pressure, *J. Fluid Contr. Fluid. Quar.* **14** (1983) (4).

- [8] P.C. Perera, N. Syred, A Coanda Switch for High Temperature Gas Control, Paper 83-WA/DSC-26, American Society of Mechanical Engineers, Winter Annual Meeting, Boston, 1983.
- [9] V. Tesař, Law governing entrainment of surrounding fluid during alternating inflow into and outflow from an orifice – in Czech, Application PO 86-84, Czechoslovak Patent Office, Prague, 1984.
- [10] G.H. Priestman and J.R. Tippetts, Development and potential of power fluidics for process flow control, *Chem. Eng. Res. Design* **62** (1984) (2), p. 67
- [11] Y. Yassour, J. Stricker and M. Wolfshtein, Heat transfer from a small pulsating jet, *Proceedings of the Eighth International Heat Transfer Conference, vol. 3*, Hemisphere Publ, San Francisco, USA (1986), pp. 1183–1186.
- [12] U. Gebhard, H. Hein and U. Schmidt, Numerical investigation of fluidic micro-oscillators, *J. Micromech. Microeng.* **6** (1996) (1), pp. 115–117.
- [13] V. Tesař, No moving part fluidic valves-in Italian, *Oleodinamica-pneumatica* **39** (1998) (3), pp. 216–223.
- [14] A. Glezer, M.G. Allen, D.J. Coe, B.L. Smith, M.A. Trautman, J.W. Wiltse, Synthetic Jet Actuators and Applications Thereof, US Patent 5,758,823 (1998).
- [15] L. Smith and A. Glezer, The formation and evolution of synthetic jets, *Phys. Fluids* **10** (1998), pp. 2281–2297.
- [16] M. Benchiekh, J.-C. Bera, M. Michard, M. Sunyach, Pulsed jet control of a short diffuser, C. R. Acad. Sci. Paris, Mécanique des fluides/Fluids Mechanics– Series IIB 328 (in French), 2000, pp. 749–756.
- [17] S.G. Mallinson, J.A. Reizes and G. Hong, An experimental and numerical study of synthetic jet flow, *Aeronaut. J.* **105** (2001) (1043), pp. 41–49. Abstract + References in Scopus | Cited By in Scopus
- [18] B.L. Smith and A. Glezer, Jet vectoring using synthetic jets, *J. Fluid Mech.* **458** (2002), pp. 1–34. [19] A. Glezer and M. Amitay, Synthetic jets, *Annu. Rev. Fluid Mech.* **34** (2002), pp. 503–529.
- [20] M. Amitay and A. Glezer, Controlled transients of flow reattachment over stalled airfoils, *Int. J. Heat Fluid Flow* **23** (2002) (2002), pp. 690–699.
- [21] J. Tensi, I. Boué, F. Paillé and G. Dury, Modification of the wake behind a circular cylinder by using synthetic jets, *J. Visual.* **5** (2002) (1), pp. 37–44.

- [22] B. Raman and A.B. Cain, Innovative actuators for active flow and noise control, *Proc. Inst. Mech. Eng. Part. G. J. Aerosp. Eng.* **216** (2002) (6), pp. 303–324.
- [23] V. Tesař and K. Peszynski, No-moving-part fluidic circulation pumps, *Proceedings of the XII ICMR Colloquium* Bydgoszcz, Poland, June (2003), p. 191.
- [24] Z. Trávníček and V. Tesař, Annular synthetic jet used for impinging flow mass-transfer, *Int. J. Heat Mass Transfer* **46** (2003), pp. 3291–3297.
- [25] V. Tesař and S. Zhong, Efficiency of synthetic jets generation, *Trans. Aeronaut. Astronaut. Soc. Rep. China* **35** (2003) (1), pp. 45–53. Abstract-Compendex | \$Order Document | Abstract + References in Scopus | Cited By in Scopus
- [26] B.L. Smith and G.W. Swift, A comparison between synthetic jets and continuous jets, *Exp. Fluids* **34** (2003), pp. 467–472.
- [27] M. Watson, A.J. Jaworski, N.J. Wood, The development of synthetic jets for enhanced control of separated flows, *Proceedings of the 33rd AIAA Fluid Dynamics Conference and Exhibition*, AIAA Paper 2003-3716, Orlando, FL, June 2003.
- [28] S. Zhong, F. Millet and N.J. Wood, The behaviour of synthetic jets in a laminar boundary layer, *Proceedings of the Seventh International Symposium on Fluid Control, Measurement, and Visualization* Sorrento, Italy, August (2003).
- [29] S.G. Mallinson, C.Y. Kwok and J.A. Reizes, Numerical simulation of micro-fabricated zero mass-flux jet actuators, *Sens. Actuators A* **105** (2003) (2003), pp. 229–236.
- [30] V. Tesař, Z. Trávníček, Pulsating and synthetic impinging jets for high heat and mass transfer rates, *Proceedings of the Seventh Biennial ASME Conference on Engineering Systems Design and Analysis ESDA 2004*, Paper ESDA2004-58236, Manchester, UK, July 2004.
- [31] Z. Trávníček, V. Tesař, A.-B. Wang, Hybrid synthetic jet actuators – numerical and experimental studies, *Sens. Actuators A: Phys.*, in press.

## Authors' Profiles

**Prof. Ing. Václav Tesař.** Received his degree in mechanical engineering in 1963 from ČVUT–Czech Technical University, Praha, Czech Republic. From 1963 to 1999 he was employed at ČVUT in Praha as Assistant, later Docent, and finally Full Professor. He received CSc degree (an equivalent of PhD) from ČVUT Praha in 1972. From 1994 to 1998 he was the Head of the Department of Fluid Mechanics and Thermodynamics, Faculty of Mechanical Engineering ČVUT Praha. In 1985, he was Visiting Professor at

Keio University, Yokohama, Japan. In 1992 he stayed as Visiting Professor at Northern Illinois University, DeKalb, USA. Since 1999 is employed as Professor the Department of Chemical and Process Engineering, Process Fluidics Group, the University of Sheffield, UK. His research interests cover shear flows, in particular jets and wall jets and their applications in fluidics for no-moving-part flow control. He is named as the inventor on 195 Czech Patents, mainly concerning fluidic devices. Recently became involved in the new field of microfluidics. He is an author of 4 textbooks and over 270 papers in various journals and conference proceedings.

**Chuan-Hsiang Hung** is a native of Taiwan. He was awarded the MSc in Environmental and Energy Engineering in 2004, for which the work reported here partially satisfied the disseration requirements.

**Dr William BJ Zimmerman** holds degrees from Princeton (BSc, Eng) and Stanford (MSc, PhD) Universities in chemical engineering. He is the recipient of five fellowships is US and UK national competitions (NSF, NATO, EPSRC and twice from the Royal Academy of Engineering). He has written over 80 scientific articles and two books: “*Process Modelling and Simulation with Finite Element Methods*” (author) and “*Microfluidics: History, Theory and Applications*” (author/editor). He is currently a Reader in Chemical and Process Engineering at the University of Sheffield and past director of the MSc in environmental and energy engineering.